GEOPHYSICS, VOL. 84, NO. 3 (MAY-JUNE 2019); P. F73–F84, 12 FIGS., 1 TABLE.
10.1190/GEO2018-0601.1

Relative source location using coda-wave interferometry: Method, code package, and application to mining-induced earthquakes

Youqian Zhao[1] and Andrew Curtis[2]

ABSTRACT

A wide range of applications requires the relative locations of sources of energy to be known accurately. Most conventional location methods are either subject to errors that depend strongly on inaccuracy in the model of propagation velocity used or demand a well-distributed network of surrounding seismic stations to produce reliable results. A new source location method based on coda-wave interferometry (CWI) is relatively insensitive to the number of seismic stations and to the source-to-station azimuthal coverage. Therefore, it opens new avenues for research, for applications in areas with unfavorable recording geometries, and for applications that require a complementary method. This method uses CWI to estimate distances between pairs of seismic events with a similar source mechanism recorded at the same station. These separation estimates are used to solve for the locations of clusters of events relative to one another within a probabilistic framework through optimization. It is even possible to find the relative locations of clusters of events with one single-channel station. Given these advantages, it is likely that one reason that the method is not used more widely is the lack of reliable code that implements this multistage method. Therefore, we have developed a well-commented MATLAB code that does so, and we evaluate examples of its applications. It can be used with seismic data from a single-station channel, and it enables data recorded by different channels and stations to be used simultaneously. It is therefore possible to combine data from permanent yet sparse networks and from temporary arrays closer to the source region. We use the code to apply the location method to a selected data set of the New Ollerton earthquakes in England to demonstrate the validity of the code. The worked example is provided within the package. A way to assess the quality of the location results is also provided.

INTRODUCTION

Finding accurate locations of seismic energy sources is essential for a wide range of seismological, industrial, and other applications. Examples include studying earthquake interaction and recurrence (Marzocchi and Lombardi, 2008; Chen et al., 2013), discriminating earthquake fault and auxiliary planes using aftershocks or foreshocks (Got et al., 1994), modeling earthquake hazards (Frankel et al., 2000), monitoring seismic activity during and after hydraulic fracturing (Kumar et al., 2017) or underground mining (Ge, 2005), and attempting to forecast earthquakes (Gerstenberger et al., 2005). In other areas of application, finding locations of different types of sources can be important; for example, in ocean acoustic (Dosso and Wilmut, 2009, 2011; Verlinden et al., 2015), in disaster rescue (Kawaguchi and Fukuda, 2017; Mae et al., 2017), and in military applications (Sheng and Hu, 2005). The quality of absolute locations found in each case depends heavily on the velocity model used, the number of stations available, and the source-to-receiver distances and azimuths. In seismological applications, earthquake location uncertainties are therefore usually of the order of kilometers or hundreds of meters, and from here on we focus only on seismological applications.

To achieve higher accuracy, relative source location methods are often used. These typically ignore absolute locations and instead estimate the locations of multiple event positions relative to each other directly from the differences in their recorded arrival times of their radiated energy at receivers that are obtained either from

Peer-eviewed code related to this article can be found at http://software.seg.org/2019/0007.
Manuscript received by the Editor 15 August 2018; revised manuscript received 14 December 2018; published ahead of production 07 February 2019; published online 29 March 2019.
[1]University of Edinburgh, School of Geosciences, Edinburgh, UK. E-mail: s1159611@sms.ed.ac.uk.
[2]University of Edinburgh, School of Geosciences, Edinburgh, UK and ETH Zurich, Department of Earth Sciences, Zurich, Switzerland. E-mail: andrew.curtis@ed.ac.uk.

catalog (preprepared) data or from temporal crosscorrelation of their various recorded waveforms (Deichmann and Garcia-Fernandez, 1992; Waldhauser and Ellsworth, 2000; Sgattoni et al., 2016). Events located in this way are often clustered within a region smaller than a quarter of the wavelength of the radiating energy at the dominant frequency; the range of source-to-receiver distances and velocity variations outside the source region therefore affect waveforms from all sources in a similar manner so that errors in their relative location associated with velocity variations are largely avoided.

Conventional relative location methods are often able to reduce seismic source relative location errors to less than approximately 100 m provided that a well-designed seismic network with a large number of stations is available (Ito, 1985; Deichmann and Garcia-Fernandez, 1992; Waldhauser et al., 1999). The master event location method (Fremont and Malone, 1987; Deichmann and Garcia-Fernandez, 1992) takes one event in an event cluster as the master event, crosscorrelates its seismogram waveforms with those of the other events, and relocates each of them relative to their master event through their relative traveltime differences. Thus, the spatial extension of the cluster is limited to about a quarter of a dominant wavelength because the waveforms of all other events need to be closely comparable with those of the master event to avoid cycle skipping in their crosscorrelation. Grigoli et al. (2016) show that the spatial extension limit can be overcome to some extent by using a multimaster event strategy if many seismic stations are available for waveform stacking. The popular double-difference (DD) location method (Waldhauser and Ellsworth, 2000; Bai et al., 2006) overcomes this limitation by linking different events and clusters using differential traveltimes obtained from catalog data, thus extending the feasible relative distance range. The DD method determines event locations by minimizing the DD (the residual between the observed and theoretical differential traveltimes of a pair of events recorded at a common station) of pair-wise events by adjusting the vector difference between their hypocenters. The system can easily become ill conditioned; hence, it is solved as a damped least-squares problem. The solution is subject to the choice of the damping factor, which depends on the condition number of the system (Waldhauser, 2001; Zhao et al., 2017). The DD location results are also influenced by the number of seismic stations available: The results deteriorate when the number falls below seven, and the method fails to produce results when the number is smaller than four (Robinson et al., 2013).

A novel location method (Robinson et al., 2013) based on coda-wave interferometry (CWI) is a feasible alternative to these conventional location methods when there are few seismic stations, or where the source-station azimuth range is unfavorable, as well as in cases in which a different method is needed for a quality check of other methods. The CWI technique (Snieder, 2006) makes use of the multiply scattered waves recorded in waveform codas that have traveled through a much larger volume of the medium and, hence, contain more azimuthal information than the first or early arrivals used by conventional methods. As a result, the CWI-based location method is even able to locate a cluster of events with one single-channel station (Robinson et al., 2013; Zhao et al., 2017).

Coda refers to the multiply scattered waves comprising the later parts of recorded seismograms, and it is extremely sensitive to differences between pairs of seismic sources (Snieder and Vrijlandt, 2005; Robinson et al., 2007) or changes in the medium of propagation (Roberts et al., 1992; Ratdomopurbo and Poupinet, 1995; Snieder et al., 2002; Gret et al., 2005, 2006). CWI measures the differences in the coda of waveforms recorded at the same station before and after some change occurs to estimate the differences between the two seismic states. For example, it has been used in a laboratory to measure changes due to the nonlinear dependence of the seismic velocity structure of granite due to temperature variations that are too small for other methods to detect (Snieder et al., 2002); to monitor velocity changes associating volcano activities (Gret et al., 2005; Wegler et al., 2006; Brenguier et al., 2008a; Baptie, 2010; Mordret et al., 2010); to study changes in fault zones (Brenguier et al., 2008b; Wang et al., 2008; de Angelis, 2009); as well as in geoengineering to monitor stress changes in concrete structures, such as bridges (Stahler et al., 2011) and buildings (Larose et al., 2006).

By comparing pairs of similar earthquakes, the source location algorithm that we present here uses CWI to estimate the intersource separations of a cluster of events with similar source mechanisms, and then it uses the separation data as the input to a location algorithm. Different types of changes in seismic states (velocity change, scatterer displacement, source displacement, and source mechanism change) leave different footprints on seismic coda when compared in a statistical manner (Snieder, 2006). Although theoretically the three types of changes could therefore be discriminated, such tests and discussion are beyond the scope of this particular work; here, we assume that differences in coda are only due to differences in the source locations of different seismic events. In such cases, clusters of events can even be located relative to one another in 3D using a single seismic receiver (Robinson et al., 2013; Zhao et al., 2017).

Despite the advantages of this method, it is curious to observe that uptake in its use has been limited to the above two papers. In part, we suspect that this is because the relative location algorithm requires unfamiliar methods to be used, and it is therefore also partly due to the lack of readily available, easily editable code with which practitioners can gain familiarity and confidence. We provide such a code.

In this paper, we present the CWI-based source location algorithm developed by Robinson et al. (2013) with the improvements proposed by Zhao et al. (2017). We then introduce a way to assess the location results obtained from the nonlinear optimization solution. We also describe the accompanying computer code, written in MATLAB, that combines these theories and methods and estimates relative source locations using a three-step routine: (1) classifying events into clusters based on waveform similarity, (2) estimating intersource separation distances with CWI, and (3) estimating the relative source locations from the separation data. In what follows, we first introduce the theory of CWI and the location algorithm in the "Estimating intersource separations with CWI" section and the "Source location" section, and then we give a brief description of the core functions and scripts of the code package in the "Code description" section. The method used to classify events (Ottemoller et al., 2017) is also described in the "Code description" section. Applications of the code to synthetic examples and to mining-induced events from New Ollerton, England, are illustrated in the "Synthetic examples" section and the "Application to New Ollerton earthquakes, England" section, respectively, and these example data sets are included within the code package.

ESTIMATING INTERSOURCE SEPARATIONS WITH CWI

CWI estimates the intersource separation between a pair of events by comparing the coda of the two seismograms recorded by each seismic station channel. The theory is based on the path summation

of scattered waves (Snieder, 1999) — the assumption that the total wavefield at a given location can be written as the superposition of waves traveling along all possible trajectories through the medium

$$u^1(t) = \sum_T A_T(t), \tag{1}$$

where $u^1(t)$ is the total wavefield from event 1, T represents a wave trajectory, and A_T is the contribution to the total wavefield of waves that travel along trajectory T. The trajectory of each scattered wave consists of the path from the source to the first scatterer encountered, and the path followed thereafter. For a second event that is close to event 1 and has a very similar source mechanism, CWI assumes that the paths to the first scatterer on each trajectory change, but that the subsequent trajectory does not because it depends on the medium rather than on the sources. Because the subsequent scattering trajectories create a complex mixture of any differences in traveltimes to the first scatters, for small changes in source location the dominant differences in recorded waveforms at the same seismic station occur in coda wave arrival times (Snieder, 2006). The wavefield of event 2 can be written as

$$u^2(t) = \sum_T A_T(t - \tau_T), \tag{2}$$

where τ_T is the traveltime difference of waves traveling along trajectory T to the first scatterer due to the difference in the source position. If we assume proximity between the two source locations and similarity in source mechanisms, and the two waveforms will be similar. Any differences can be quantified by the normalized crosscorrelation of the two waveforms in a time window defined by a central time t and a half-width t_ω computed for a sequence of time windows in the coda

$$R(t_s) = \frac{\int_{t-t_\omega}^{t+t_\omega} u^{(1)}(t')u^{(2)}(t'+t_s)dt'}{\sqrt{\int_{t-t_\omega}^{t+t_\omega} u^{(1)^2}(t')dt' \int_{t-t_\omega}^{t+t_\omega} u^{(2)^2}(t')dt'}}. \tag{3}$$

The distribution of any traveltime differences τ_T in each time window contains information about the source separation δ. Snieder (2006) estimates the standard deviation of the traveltime difference φ_τ from the maximum of the correlation coefficient $R_{\max}$, and it shows that φ_τ is related to the source separation δ by

$$\varphi_\tau^2 = \frac{1}{2}\frac{\delta^2}{v^2} \tag{4a}$$

for isotropic sources in 2D acoustic media,

$$\varphi_\tau^2 = \frac{1}{3}\frac{\delta^2}{v^2} \tag{4b}$$

for isotropic sources in 3D acoustic media, and

$$\varphi_\tau^2 = \frac{6/\alpha^8 + 7/\beta^8}{7(2/\alpha^6 + 3/\beta^6)}\delta^2 \tag{4c}$$

for double couple sources on the same fault plane.

Here α and β are the P- and S-wave velocity in the vicinity of the two sources (Snieder and Vrijlandt, 2005). The waves arriving in different time windows have traveled along different paths, so separation results derived from each time window of the seismograms are therefore independent and their distribution can be used to estimate uncertainty. It has also been shown that estimates of inter-source separations from different station channels are highly consistent (Snieder and Vrijlandt, 2005; Robinson et al., 2011; Zhao et al., 2017). Note we have assumed that the difference in the two waveforms is only due to the second event having a different location than the first; however, in reality the change in source location may be accompanied by a velocity change or scatterer displacement in the medium of propagation. In cases in which other types of changes also occur, the estimation of source separations would be overestimated, especially for event pairs with small source separations because all perturbations contribute negatively to the correlation coefficient (equation 3), hence positively to the source separation estimates (equation 4).

As we move through a seismogram toward later times, the seismic coda becomes suitable for CWI in which the waves are sufficiently scattered so that a time window contains waves leaving the source from many different directions; the suitable section ends where the noise level exceeds that of the signal. Therefore, there is a limited length of coda that can be used. In turn, this constrains the choices of the number and length of time windows used in equation 3, and clearly there is a trade-off between the two. From a theoretical point of view, if we insert wave representations 1 and 2 into equation 3, we can see that computation of $R(t_s)$ gives rise to double sums. CWI assumes that the cross terms between the two summations are negligible compared with the diagonal terms, but their ratio is inversely proportional to the length of the time windows (Snieder, 2006). Hence, for this assumption to be reasonable, the time windows need to have sufficient length. However, time windows cannot be unrestrictedly long; otherwise, cycle skipping may occur in the crosscorrelation in equation 3. Also, to obtain usable standard deviations on separation estimates, at least four time windows are needed for each pair of waveforms. Given all of these constraints, it is not a trivial task to select the number, length, and start time of the windows used to implement CWI.

To avoid the vagaries of trial and error, the code package allows the separation-uncertainty matrix of Zhao et al. (2017) to be used to find the most suitable combination of the number, length, and start time of windows systematically. For data from each station channel, a 3D separation-uncertainty matrix is computed that includes a regularly sampled subset of all possible combinations of the three parameters: the number, length, and start time of the windows. Matrix elements are computed for one combination of the three parameters by first calculating $\Omega_{i,j} = \sum_N \sigma_{i,j}/N$, where $\sigma_{i,j} = \sqrt{\sum_{k=1}^{l}(\delta_{i,j,k} - \bar{\delta}_{i,j})^2/l}$ is the standard deviation of the separation estimates from l coda time windows for events i and j, $\delta_{i,j,k}$ is the separation estimate from the kth window, $\bar{\delta}_{i,j}$ is the mean separation over l windows, and N is the number of event pairs on that station channel. The value of $\Omega_{i,j}$ reflects the uncertainty of separation estimates derived from one recording channel for each source pair. Averaging over all source pairs gives a final uncertainty estimate for that combination of parameters. Thus, systematically searching for the combination of number, length, and start time of windows that gives the lowest estimate of separation uncertainties from CWI becomes an automated process.

It is essential to note that the CWI technique has a tendency to underestimate larger source separations due to cycle skipping in the correlation of coda in equation 3. This trend can be quantified by two empirical relations between the true separation $\tilde{\delta}_t$ and the mean $\mu = \mu(\tilde{\delta}_t)$ and standard deviation $\sigma = \sigma(\tilde{\delta}_t)$ of CWI separation

estimates (Figure 1a and 1b), where the tilde above the separation indicates that the quantity is normalized by the dominant wavelength λ_d in the recorded data: $\tilde{\delta}_t = \delta_t/\lambda_d$. The applicable range of CWI is visualized in Figure 1: CWI fails to identify any increase in length when the true separation is larger than $0.55\lambda_d$. The empirical functions that capture this behavior are derived from a multitude of synthetic experiments with a large range true separations in different Gaussian random media, by fitting the rational functional forms

$$\mu(\tilde{\delta}_t) = a_1 \frac{a_2 \tilde{\delta}_t^{\,a_4} + a_3 \tilde{\delta}_t^{\,a_5}}{a_2 \tilde{\delta}_t^{\,a_4} + a_3 \tilde{\delta}_t^{\,a_5} + 1}, \tag{5a}$$

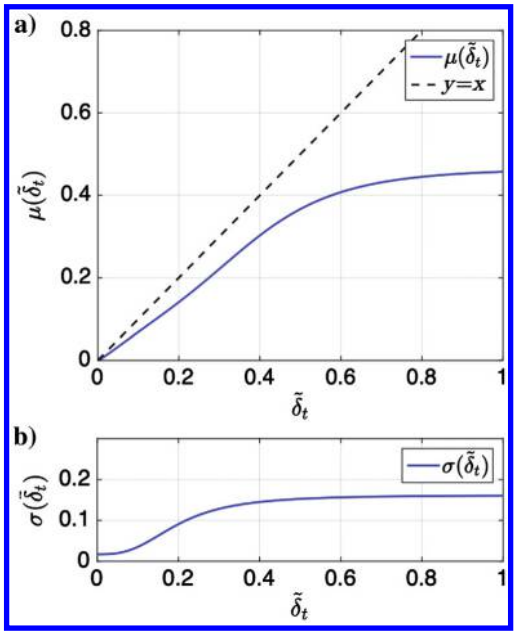

Figure 1. Empirical functions showing the bias and uncertainties in separation estimates from the CWI technique. (a) The empirical relation between the mean of the source separation estimates $\mu = \mu(\tilde{\delta}_t)$ and the true separation $\tilde{\delta}_t$. All separations are normalized by the dominant wavelengths of the coda waveforms. The dashed line $y = x$ shows the case in which the mean of the CWI separation estimates is identical to the true separations. (b) The empirical relation between the standard deviation $\sigma(\tilde{\delta}_t)$ of the separation estimates and the true separation $\tilde{\delta}_t$.

Table 1. Constants in the empirical relations in equation 5a and 5b for $\mu = \mu(\delta_t)$ and $\sigma = \sigma(\delta_t)$ (Robinson et al., 2013).

$\mu = \mu(\tilde{\delta}_t)$	$\sigma = \sigma(\tilde{\delta}_t)$
$a_1 = 0.4661$	$b_1 = 0.1441$
$a_2 = 48.9697$	$b_2 = 101.0376$
$a_3 = 2.4693$	$b_3 = 120.3864$
$a_4 = 4.2467$	$b_4 = 2.8430$
$a_5 = 1.1619$	$b_5 = 6.0823$
—	$c = 0.017$

$$\sigma(\tilde{\delta}_t) = b_1 \frac{b_2 \tilde{\delta}_t^{\,b_4} + b_3 \tilde{\delta}_t^{\,b_5}}{b_2 \tilde{\delta}_t^{\,b_4} + b_3 \tilde{\delta}_t^{\,b_5} + 1} + c, \tag{5b}$$

where the values of the constants are listed in Table 1 (Robinson et al., 2011, 2013). The location algorithm introduced in the next section takes account of these known biases of CWI-estimated source separations, and it is able to correct for them to a significant extent in relative location results.

SOURCE LOCATION

The source location algorithm estimates the relative locations from the separation estimates and their uncertainties using a probabilistic framework. Robinson et al. (2011) describe the probabilistic nature of CWI estimates using the conditional probability density function (PDF) $P(\tilde{\delta}_t|\tilde{\delta}_{\mathrm{CWI}})$, which is the probability of the true separation being $\tilde{\delta}_t$ given that the estimate from CWI is $\tilde{\delta}_{\mathrm{CWI}}$. According to Bayes' theorem, this so-called posterior probability of $\tilde{\delta}_t$ is proportional to the likelihood of observing $\tilde{\delta}_{\mathrm{CWI}}$ in the case that the true separation is $\tilde{\delta}_t$, multiplied by the prior probability of $\tilde{\delta}_t$ being true

$$P(\tilde{\delta}_t|\tilde{\delta}_{\mathrm{CWI}}) \propto P(\tilde{\delta}_{\mathrm{CWI}}|\tilde{\delta}_t) \times P(\tilde{\delta}_t). \tag{6}$$

The prior PDF $P(\tilde{\delta}_t)$ is used to describe information about the source separation or event location known prior to and independently from the CWI location process, which here is considered to be a uniform distribution with wide bounds. The likelihood function $P(\tilde{\delta}_{\mathrm{CWI}}|\tilde{\delta}_t)$ is approximated by a positively bounded Gaussian PDF, whose mean and standard deviation are, respectively, represented by the empirical functional relation $\mu(\tilde{\delta}_t)$ and $\sigma(\tilde{\delta}_t)$, given true separation $\tilde{\delta}_t$.

For a cluster of events, equation 6 holds for each event pair. Robinson et al. (2013) incorporate the separations between multiple event pairs by multiplying the formulas for all available event pairs to establish their joint posterior PDF, assuming that they are independent of each other

$$P(\mathbf{e}_1, \ldots, \mathbf{e}_n|\tilde{\delta}_{\mathrm{CWI}}) = c \prod_{i=1}^{n} P(\mathbf{e}_i) \times \prod_{i=1}^{n-1} \prod_{j=i+1}^{n} P(\tilde{\delta}_{\mathrm{CWI},ij}|\mathbf{e}_i, \mathbf{e}_j), \tag{7}$$

where c is a constant, n is the number of events, and $\mathbf{e}_i = (x_i, y_i, z_i)$ is the location of event i. Within the last term, we use the Euclidean distance $\delta_{\mathrm{CWI},ij} = \mathbf{e}_i - \mathbf{e}_{j2}$ for source separation between the ith and jth earthquakes. Throughout the evaluation of the joint PDF, the separation quantities are used in normalized form; that is, they are divided by the dominant wavelength λ_d. However, the dominant frequency, and hence the dominant wavelengths of the set of events, could extend over a large range, and it is also subject to the limitations of the recording instruments. Using the average dominant wavelength over different station channels therefore introduces inaccuracy to the location process. To this end, our code package instead uses the joint PDF introduced by Zhao et al. (2017), which applies an individual likelihood for each channel when data from multiple channels are used, so that the separations computed during

the evaluation of the joint PDF are normalized by the actual dominant wavelength from that channel,

$$P(\mathbf{e}_1, \ldots, \mathbf{e}_n|\tilde{\delta}_{\mathrm{CWI}}) = c\prod_{i=1}^{n} P(\mathbf{e}_i) \times \prod_{k=1}^{m}\prod_{i=1}^{n-1}\prod_{j=i+1}^{n} P_k(\tilde{\delta}^k_{\mathrm{CWI},ij}|\mathbf{e}_i, \mathbf{e}_j), \quad (8)$$

where m is the number of channels used, k is the index over m channels, and $P_k(\tilde{\delta}^k_{\mathrm{CWI},ij}|\mathbf{e}_i, \mathbf{e}_j)$ is the probability of observing $\tilde{\delta}^k_{\mathrm{CWI},ij}$ given source locations $\mathbf{e}_i$ and $\mathbf{e}_j$, where $\tilde{\delta}^k_{\mathrm{CWI},ij}$ is normalized by the dominant wavelength of the kth channel. The maximum of the joint posterior PDF (equation 8) occurs at the most probable combination of event locations. Hence, the event locations can be estimated by solving an optimization problem. Taking the negative logarithm of equation 8, the multiplications are converted to summations that are more numerically stable:

$$-\ln[P(\mathbf{e}_1, \ldots, \mathbf{e}_n|\tilde{\delta}_{\mathrm{CWI}})] = -\ln[c] - \sum_{i=1}^{n}\ln[P(\mathbf{e}_i)] - \sum_{k=1}^{m}\sum_{i=1}^{n-1}\sum_{j=i+1}^{n}\ln[P_k(\tilde{\delta}_{\mathrm{CWI},ij}|\mathbf{e}_i, \mathbf{e}_j)]. \quad (9)$$

Maximization of equation 8 is equivalent to minimizing equation 9, where $\ln[c]$ and $\ln[P(\mathbf{e}_i)]$ can be ignored because they are constant (for uniform priors). Thus, the event locations $\mathbf{e}_1, \ldots, \mathbf{e}_n$ can be found by minimizing the objective function:

$$L(\mathbf{e}_1, \ldots, \mathbf{e}_n) = -\sum_{k=1}^{m}\sum_{i=1}^{n-1}\sum_{j=i+1}^{n}\ln[P_k(\tilde{\delta}_{\mathrm{CWI},ij}|\mathbf{e}_i, \mathbf{e}_j)]. \quad (10)$$

In the code package, objective function L is minimized using a conjugate gradient method, the Polak-Ribiere technique (Navon and Legler, 1987; Press et al., 1987).

CODE DESCRIPTION

The accompanying relative source location code is written in MATLAB with well-commented functions and scripts. These use seismic data recorded with single or multiple station channels to find relative source locations. The package consists of three parts, each of which contains codes conducting one step of the location method: clustering events, estimating intersource separations, and estimating source locations. The entire process can be implemented by executing the script `main_running_script.m` section by section, with interactive operations involved occasionally. This section provides descriptions of the core functions and scripts used in each step. The sub and auxiliary functions and scripts are explained in the user guide that is included within the package.

Clustering

The theory of CWI requires that events be constrained to have identical source mechanisms, so events first need to be classified into sets of similar mechanism. The similarity in pairs of sources is assessed by the similarity of their waveforms recorded by the same seismic station channel, which is measured by their crosscorrelation. The package classifies events in two steps, computing crosscorrelations then identifying clusters, with scripts `sort_cr.m` and `clustering.m`, respectively.

The script `sort_cr.m` reads in seismic data in seismic analysis code (SAC) form (Helffrich et al., 2013). It first selects events and station channels for location according to criteria set by the user: `MIN_channel` is the minimum number of recording channels for an event to be considered, and `MIN_event_per_channel` is the minimum number of events recorded by a channel for that channel to be used. It then calculates the normalized crosscorrelation $R(t_s)$ of all available pairs of the selected events recorded by each selected station channel, and it finds the maximum of each crosscorrelation $R_{\max}$. For each event pair, the values of $R_{\max}$ are averaged over all selected station channels that have recorded both events, then these average maximum crosscorrelation $\mathrm{cravg}_{\max}$ are sorted in descending order.

The script `clustering.m` follows the method of Ottemoller et al. (2017) to identify clusters. It starts with the event pair with the highest $\mathrm{cravg}_{\max}$ value, making them the first two events of the first cluster. It then searches through the sorted list of $\mathrm{cravg}_{\max}$, adding events that are linked to the current cluster. A link to a cluster is defined as one of the events in the pair being correlated ($\mathrm{cravg}_{\max}$ higher than `MIN_corr`, the threshold of $\mathrm{cravg}_{\max}$ for an event pair to be included) with any event that is already in the cluster. The search restarts from the first unclassified pair (the unclassified pair with the highest $\mathrm{cravg}_{\max}$) every time a new event is added to the cluster to avoid overlooking any linked events. The search loops until there is no event that can be added to the current cluster, after which it starts a new cluster from the two events of the first unclassified pair in the sorted list. The search ends when all events are classified. Clusters with fewer then `MIN_E_per_CLUSTER` events will not be identified as being part of a cluster.

Estimating intersource separations

For each identified cluster, seismic data are processed in three substeps to estimate intersource distances: picking waveform first arrivals; determining the combination of number, length, and start time of windows for implementing CWI; and estimating source separations with CWI. Users are free to conduct first-arrival picking with their preferred method; however, this package provides a user-friendly way for the task to be carried out in a graphical, interactive manner. The core functions and scripts are as follows:

1) `first_arrival_pick.m`: This is a script that allows users to pick the first arrivals of a series of waveforms interactively.
2) `separation_parameters.m`: This is a script that finds the combination of number, length, and start time of windows to implement CWI with CWI_sep.m (see below) that gives the lowest separation uncertainties.
3) `separations.m`: This is a function that estimates the intersource separations of all event pairs in a given cluster recorded by a given station channel.
4) `CWI_sep.m`: One of the core functions in the package called by multiple functions and scripts. It applies CWI (Snieder, 2006) to estimate the separation between one pair of sources with similar mechanisms for isotropic sources in a 2D or 3D acoustic medium, or double-couple sources in an elastic

medium (Snieder and Vrijlandt, 2005). The two improvements introduced by Robinson et al. (2011) are applied: (1) removing the Taylor series approximation of the waveform autocorrelation and (2) applying a restricted range when searching for the maximum correlation value $R_{\max}$ to avoid cycle skipping.

The result of applying these functions is a data set of intersource separations estimated by CWI, which are ready to be used to estimate relative source locations.

Estimating source locations

The relative locations of a cluster of events are solved by minimizing the objective function L (equation 10). To start the minimization, a set of initial event locations is needed, which can either be generated with function `initialize_locations.m` in the package or can be provided by user. The main location function `Source_Location.m` first evaluates L at the given initial event locations and computes its gradient, whose negative is the steepest descent direction and is used as the initial search direction. The function searches for the minimum along the search direction using a two-tier line search algorithm by calling `line_search.m`. First, this routine conducts a brute-force search by evaluating the objective function at regularly spaced points within a bracketed range to find bounds on a finer range search, and then it conducts a second similar brute force search to find the approximate minimum within those bounds, and finally sharpens the result by fitting a parabola using the approximate minimum and an adjacent point on each side. The event locations are then updated to the minimum found, and the value of L is reduced. The function then calculates the next search direction, a direction orthogonal to the gradient at the current position and conjugate to the last search direction, finds the minimum along the new search direction, and updates the event locations. This process iterates until one of three conditions is met: (1) the value for any nonzero step length is larger than that obtained in the previous iteration, (2) the reduction in the value of L in an iteration is smaller than a threshold, or (3) the maximum allowed number of iterations is reached. Starting with a different set of initial locations is recommended if the iterations are terminated due to the third criterion because some initializations may lead to convergence more rapidly than others.

For this part of the method, the core functions and scripts are

1) `Source_Location.m`: This is the main location function that estimates the relative location of a cluster of events using intersource separation data (their mean and standard deviations) estimated with CWI.
2) `ln_joint_likelihood.m`: This is a function that evaluates function L (equation 10) — the negative logarithm of the joint likelihood function for a cluster of events.
3) `gradient.m`: This is a function that computes the gradient of function L numerically at a given set of event locations.
4) `line_search.m`: This is a function that searches for the minimum of a 1D function along a given direction.
5) `initialize_locations.m`: A function that generates a set of initial locations for the minimization. It first randomly generates a set of locations, and then it adjusts the order of these event locations to conform as well as possible to the input CWI separation estimates (so as to ensure the smallest sum of square residuals between the source separations given by the initial event locations and the mean of CWI separation estimates). This reordering procedure moves the initialization of optimization closer to the minimum, thus improving the speed of convergence.
6) `rotate_cluster.m`: This is a function that rotates a cluster of points about its center in two orthogonal directions in the 3D space by given angles.

SYNTHETIC EXAMPLES

We use synthetic experiments to demonstrate the validity of the method and code; the data for these experiments are included in the code package so that users can verify their version of codes after editing to fit their specific needs. Applications of intersource separation estimation and source location are shown separately in this section to identify the abilities and limitations of each of the two successive steps. Whereas the theory of CWI assumes point scatterers (Snieder, 2006) with a constant background velocity, we use the Marmousi 2 model (Martin et al., 2002; Irons, 2005) to test the method in a more realistic representation of earth's velocity structure. The Marmousi 2 model is an elastic extension of the classic Marmousi model (Versteeg, 1994), which is based on a profile though the North Quenguela trough in the Cuanza Basin and contains a large number of horizontally layered horizons and a series of normal faults. The new model also has more structural complexities and structural features compared with the original; hence, it is used in our example. We then demonstrate the performance of the optimization algorithm used to solve for event locations using CWI separation estimates. In the subsequent section, we apply all three steps in the method (clustering, CWI, and source location) to real earthquake data.

Estimating intersource separations

We modeled the waveforms from two identical isotropic sources in the Marmousi 2 model (Figure 2), which has an average velocity of 1250 m/s. The recording network consists of a surface array with 15 receivers and two borehole arrays with 12 receivers each. The two sources are 64.7 m apart with a dominant frequency of 5 Hz, and the dominant wavelength λ_d of the waveforms is 250 m. We apply the function `CWI_sep.m` to obtain estimates of the separation between the two sources. The estimates from different time windows fluctuate around their mean at narrow distances as shown in Figure 2b for receiver R1, which gives a mean of 59.15 m and a standard deviation of 6.40 m. This result agrees with the empirical relations (Figure 1) that for a true separation $\delta_t = 64.7$m (i.e., $\tilde{\delta}_t = 0.259\lambda_d$), the separation mean $\mu(\delta_t)$ and standard deviation $\sigma(\delta_t)$ are estimated to be $0.237\lambda_d$ and $0.026\lambda_d$. The separation estimates are consistent among different receivers in the surface array and borehole arrays, with uncertainties similar to that given by the empirical relations as shown in Figure 2c. For most receivers, the true separation is contained within one standard deviation of the mean of their associated separation estimates.

Estimating source locations

To demonstrate the ability of the code to solve for locations of a cluster of events using CWI separation estimates, we randomly distribute 50 sources in a cube with side length of 300 m, shown as the hollow circles in Figure 3. The dominant wavelength is $\lambda_d = 534$m, and the maximum source separation $\lambda_{\max}$ is 424m (i.e., $0.8\lambda_d$).

For the purpose of this example, we create CWI separation data (separation mean and standard deviations) using the empirical relations (equation 5), where the true separations are computed as $\delta_t = \sqrt{(x'-x)^2 + (y'-y)^2 + (z'-z)^2}$ for events $e = (x, y, z)$ and $e' = (x', y', z')$. The separation data are thus exactly consistent with the known biases and level of uncertainty of the CWI technique so that in this example we isolate the performance of the optimization algorithm that estimates the source locations.

To implement the location process, initial locations for the 50 events are randomly distributed within the 3D cube using `initialize_locations.m` as shown in Figure 3a. Thereafter, the optimization took 27 iterations to converge with estimated locations shown as the solid circles in Figure 3b. The improvement in event locations from the optimization is readily observed by comparing the result with their initial locations (the red triangles in Figure 3a). The optimization does not lead the estimated locations to exactly the true event locations, due to the uncertainty $\sigma(\tilde{\delta}_t)$ in the separation data used. The average location error is 27 m, corresponding to $0.05\lambda_d$. Figure 4 compares source separations calculated from the relocated event locations (red) to the separation data (blue) used as input to the optimization. This shows that although the input separation data deviate significantly from their actual value (the dashed line $y = x$) where the true separation is larger than $0.55\lambda_d$, the recovered source separations are only slightly underestimated. Thus, it is proven that the location algorithm is able to correct biases in the CWI estimates to a large extent.

Optimization techniques that guarantee convergence to the global minimum of a complicated nonlinear objective function do not currently exist. To this end, we implement the optimization multiple times with different random initializations of event locations. We illustrate the change of objective function value during the optimization process for all implementations in Figure 5. The six optimizations start with different objective function values because of their different random initial event locations. The value decreases rapidly for the first 10 iterations and then slows down as the algorithm approaches the various minima. All cases converge to the same minimum of 6738, except for the fourth, which gets stuck at a local minimum of 6753. For this synthetic example, the true (global) minimum of the objective function is known because the true event locations are known, and we find that error in the minimum found when optimization is below 1, which is negligible.

However, when applying the algorithm to real events in which the correct minimum is unknown, using several optimizations from random event initializations can add confidence to the result to which most implementations converge.

APPLICATION TO NEW OLLERTON EARTHQUAKES, ENGLAND

New Ollerton, near Nottingham, England, is a region where historical (micro-) seismic activity is related to coal mining. After some small earthquakes were detected, the British Geological Survey (BGS) deployed a temporary recording network in early 2014 to monitor further activities (Figure 6). These events have magnitude of 0.7–1.8 ML, and the waveforms in standard SAC

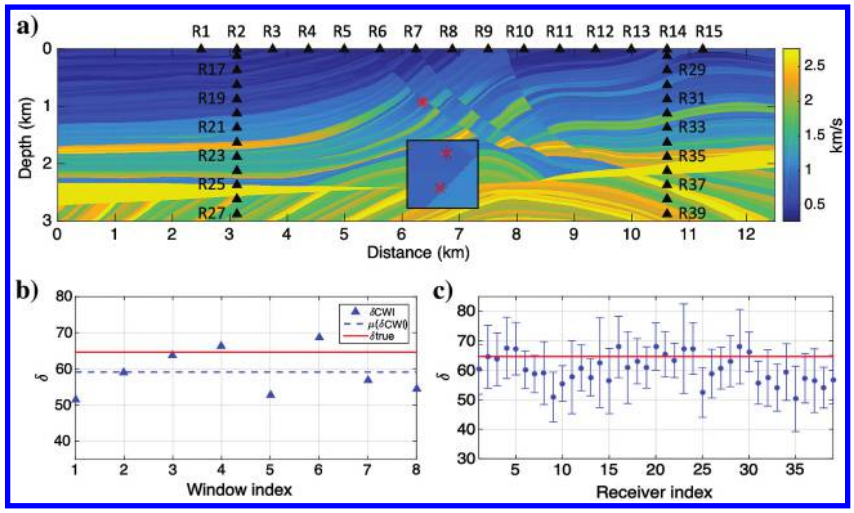

Figure 2. (a) The Marmousi 2 S-wave velocity model (Irons, 2005) used for the synthetic example. The triangles and stars are the receivers and sources, respectively; the small square shows the source region magnified. (b) The separation estimates (triangles) of each time window from receiver R1 only, with the mean indicated by the dashed line and the true separation between the two sources by the solid line. (c) Separation estimates from all individual receivers with error bars showing the mean plus/minus one standard deviation; the red line is the true separation between the two events.

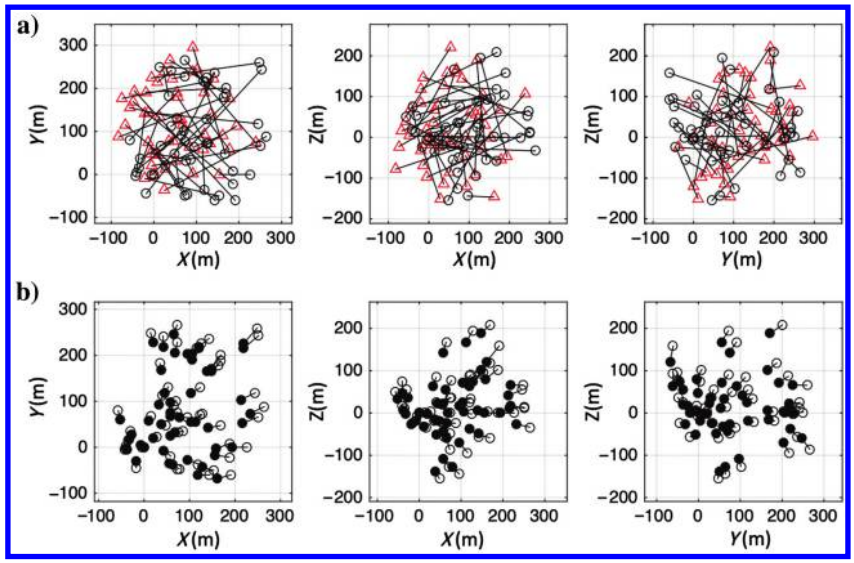

Figure 3. Planar projections of event locations, where axes x, y, and z point in three orthogonal directions. (a) Comparison of the events' actual locations (circles) and their initial locations (triangles) before optimization, and the black bars show their differences. (b) The events' actual locations (the hollow circles) and the location results obtained (the solid circles), with lines between the hollow and solid circles representing postoptimization location errors.

format (Helffrich et al., 2013) are filtered to 2–20 Hz. Our data set contains 118 SAC files, with 41 events recorded by five different channels of seismic stations. The code allows users to set customized criteria for selecting events and channels to be used to estimate locations. In this example, we required that events have been recorded by at least two station channels to be considered for clustering and then for location in the later steps. We also required that only station channels that have recorded at least 10 events contained in the total data set (all 118 SAC files) should be used. These criteria are to ensure the robustness of the data chosen for source location, presuming that having fewer data of higher quality gives more reliable results than more data of inconsistent quality. As a result, 34 events and three channels (channels NOLCZ, NOLFE, and NOLFN) are selected to be used for the source location based on the above criteria.

With the threshold on the correlation coefficient of linked events set to `MIN_corr=0.9`, and the minimum number of events to form a cluster set to five, the selected events are classified into two clusters with 11 and 23 events, respectively, with no unclassified events. Note that setting `MIN_corr` to 0.9 does not ensure that all events classified as being in the same cluster have an average maximum correlation coefficient $\text{cravg}_{\text{max}}$ over all station channels with one another; rather, it ensures that each event in a cluster has a $\text{cravg}_{\text{max}} \geq 0.9$ with at least *one* other event in the same cluster. Hence, it is recommended to set a high `MIN_corr` to ensure a sufficient level of waveform similarity for CWI to be applied. Figure 7a shows the waveform correlation matrix of 23 events in cluster 2 recorded by station channel NOLFN, there are some waveform pairs whose R_{max} is very close to one, whereas the lowest R_{max} in the cluster is only slightly greater than 0.6. Figure 7b and 7c shows comparisons of waveform pairs with the highest and lowest R_{max}, respectively.

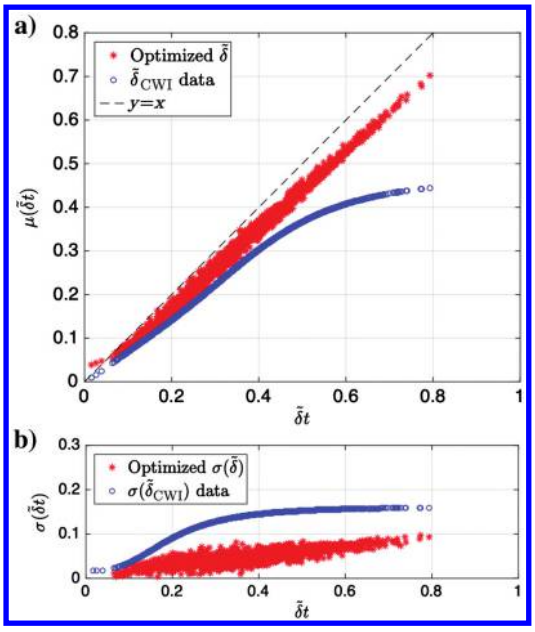

Figure 4. A comparison of input intersource separations (the blue circles) and separations calculated from the location result after optimization (the red asterisks). (a and b) The separation data and their standard deviations, respectively.

For each cluster and each selected channel, we use the separation-uncertainty matrix to find the combination of number, length, and start time of windows that give the lowest uncertainties of CWI separation estimates. For example, for cluster 1 recorded by channel 1 (NOLCZ), the lowest average uncertainty of separation estimates is $\Omega = 11.08$ m, when using four time windows with a length of 2.5 s, starting from 19 s, indicated by the darkest blue grid cell at the bot-

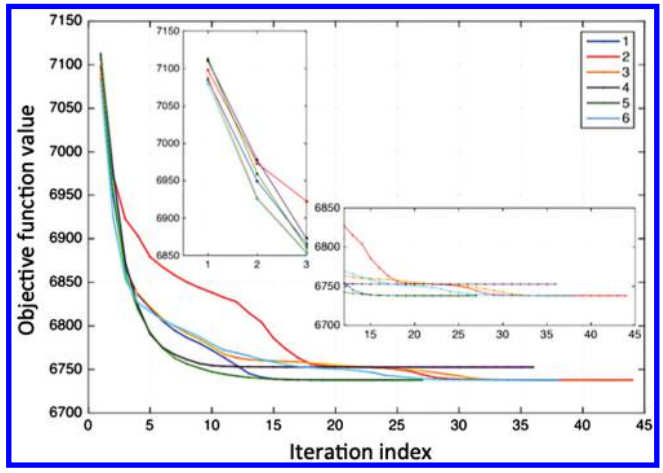

Figure 5. Illustration of the minimization process of each optimization from different initializations of random event locations using different colors to indicate each example optimization. The magnified panels show details of how the values of the objective function change with the iteration number at the beginning and end of each optimization. The objective function is given in equation 10.

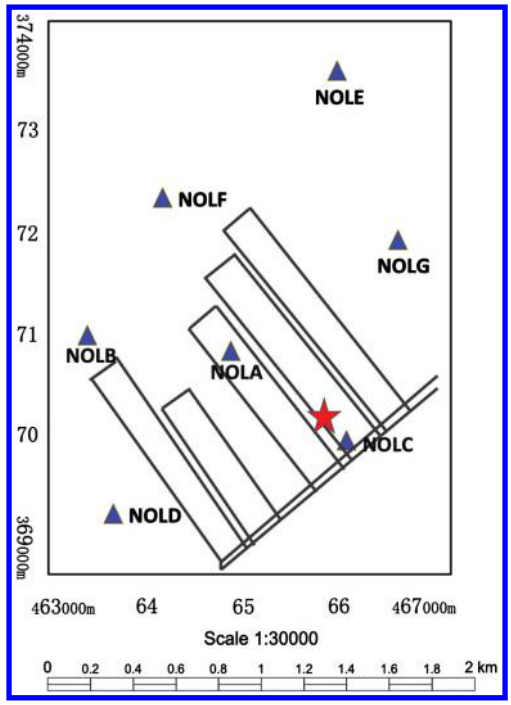

Figure 6. Map of the source region near Thorsby colliery, New Ollerton, Nottinghamshire, England. The rectangles indicate the locations of subsurface mining galleries, the star shows the area where the microearthquakes are likely to have occurred, and the triangles are the temporary seismic stations.

tom left of Figure 8. The separation-uncertainty matrix provides a guideline to choose an appropriate combination of parameters to use for CWI. Usually, we find that when using other combinations of parameters, the results do not change significantly as long as we do not deviate too far from the optimal values found from the matrix.

We estimated source locations for each cluster using separation estimates obtained from all channels and from individual channels. For each location optimization, 10 different random initializations are used to evaluate the robustness of our location results. Figure 9a and 9b shows the progress of each implementation of clusters 1 and 2 using data from channel NOLCZ, with the horizontal magnified panels showing details of the eventual convergence. All cases converged to similar levels to within reasonable numerical errors. The convergence for cluster 2 seems less consistent than those for cluster 1. This is as expected: Cluster 1 contains 55 event pairs from 11 events; hence, its objective function L involves the sum of the logarithm of 55 pair-wise likelihood functions (equation 6), whereas cluster 2 comprises 23 events so function L involves the sum of the logarithm of 253 pair-wise likelihood functions. The consistent convergence level suggests that the minimum found using different random initializations should be close to the global minimum of function L; therefore, the relative source locations have been found.

The intersource separations obtained from the optimizations are consistent among individual channels (red, blue, and green) with small residuals, and they are very similar to the results obtained using all three channels (black) as shown in Figure 10a. The location process corrects for the underestimation bias of the CWI technique, as we see by comparing the recovered separations (red) and the original CWI separation data (black) used as the input to the optimization (Figure 10b). Figure 11 illustrates the location results of cluster 2 using data from individual channels and data from all three channels, projected onto three orthogonal planes. The patterns show a high level of consistency among single channels and multiple channels. All channel combinations predict a characteristic horseshoe-type structure for the cluster. Thus, we show once again that the CWI source location technique is able to give reliable relative location estimates even from single recording channels. For comparison, the DD location result using data from 11 available seismic station channels is shown in Figure 12, in which the two methods constrain the events to a similar level of clustering.

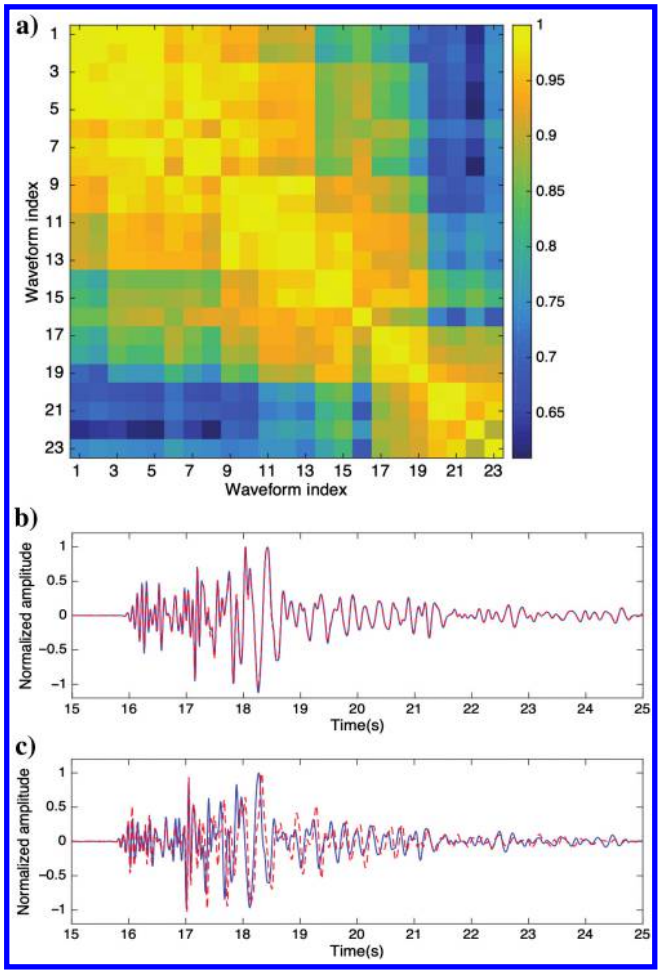

Figure 7. Illustration of waveform similarity. (a) The correlation matrix of waveforms of the 23 events in cluster 2 recorded by station channel NOLFN. Each cell represents the maximum of correlation coefficient R_{max} of the corresponding event pair, whose value is indicated by the cell color. (b and c) The waveform pair with the highest and lowest R_{max}, respectively.

DISCUSSION

A wide range of seismic applications requires accurate relative source locations. The popular DD method (Waldhauser and Ells-

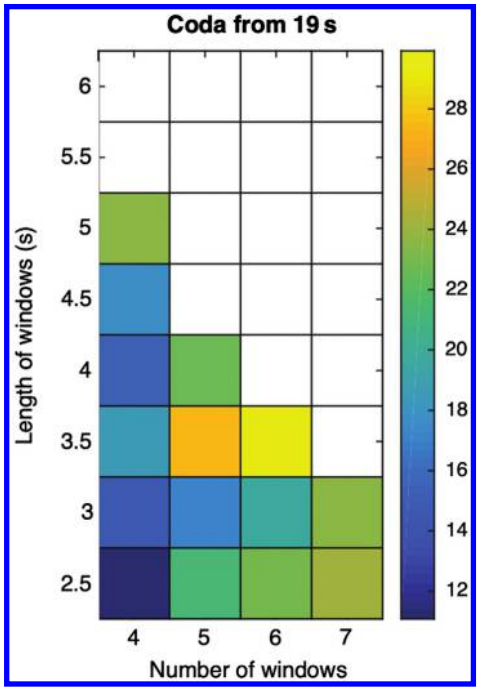

Figure 8. A slice of the 3D separation uncertainty matrix. The colors indicate the values of the average standard deviations resulting from the corresponding parameter combination of number of windows, window length, and start time of the windows, used to divide the coda. The white cells indicate parameter combinations that are not supported by the available data. For all scenarios represented in this slice, the start of the time windows is 19 s. The parameter combination giving the lowest average separation uncertainty is four windows with a length of 2.5 s, starting from 19 s.

worth, 2000) produces high-resolution location results when a large number of seismic stations are available; however, its performance deteriorates when this requirement is not met, and results are subject to the choice of damping factor when solving the least-squares problem. The novel location method based on CWI opens a new avenue for research and applications in areas where a dense recording system with good source-station azimuthal coverage is unavailable or where an independent method is useful to test the compatibility of the robustness of existing methods.

Although we have developed and used the code package for seismic applications, there are numerous other areas in which energy source location estimates are useful or necessary as summarized in the "Introduction" section of this paper. The CWI method could potentially be applied to any of them, provided that the medium of wave-propagation scatters the wavefield strongly in many directions. This is necessary to ensure that the recording of coda at each receiver contains energy that left each source at a wide range of angles. This range of angles is the equivalent of the standard requirement of a wide aperture between each source and the set of receivers for conventional location methods. However, the equivalence is not direct because all of the latter methods use deterministic physics to optimize locations by matching synthetic and real data, whereas CWI uses statistical (nondeterministic) relations to estimate source separations. This difference means that CWI can also be used to provide an independent test of the efficiency of other source location methods, and also that CWI uses far more recorded data than these methods.

The CWI-based method was first developed approximately 10 years ago (Snieder and Vrijlandt, 2005; Robinson et al., 2011) but the uptake of the method has been slow, with only two known applications to earthquake location (Robinson et al., 2013; Zhao et al., 2017). This may partly be explained by the lack of a readily available code package to implement the method, a deficiency that we rectify herein. Harder is to change the attitude that seismologists know the structure of the medium (earth) well enough that deterministic methods can be used. Indeed, CWI as used here takes the opposite view: that we do not know the structure well because the existence of strong coda in most recordings of crustal earthquakes shows that there must be strong scattering from unknown structures. The examples presented here show that even in such cases, relative locations can be found over length scales of a fraction of a wavelength, which should go some way toward convincing others that this point of view is valid and useful.

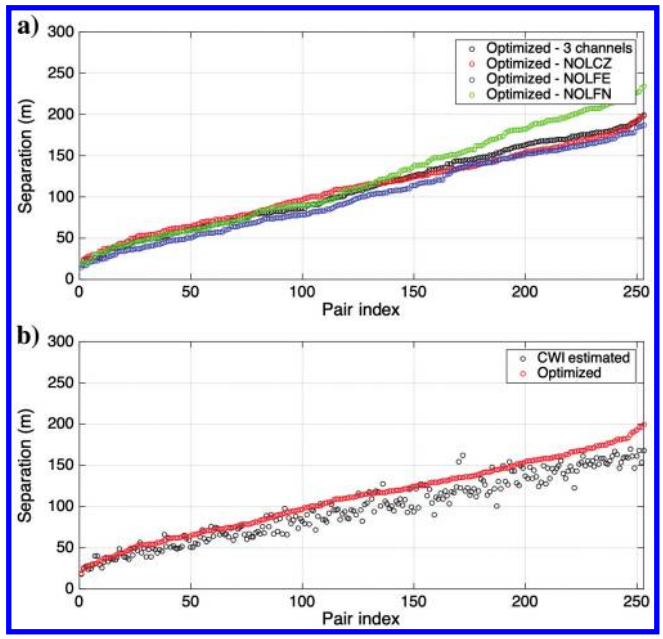

Figure 10. CWI estimates of source separations and their optimized counterparts (the latter are calculated from the estimated event locations) of cluster 2. (a) The optimized separations using all three channels (black) and using single channels NOLCZ, NOLFE, and NOLFN (red, blue, and green). (b) Compares the optimized separations of channel NOLCZ (red) with the original CWI separation estimates (black).

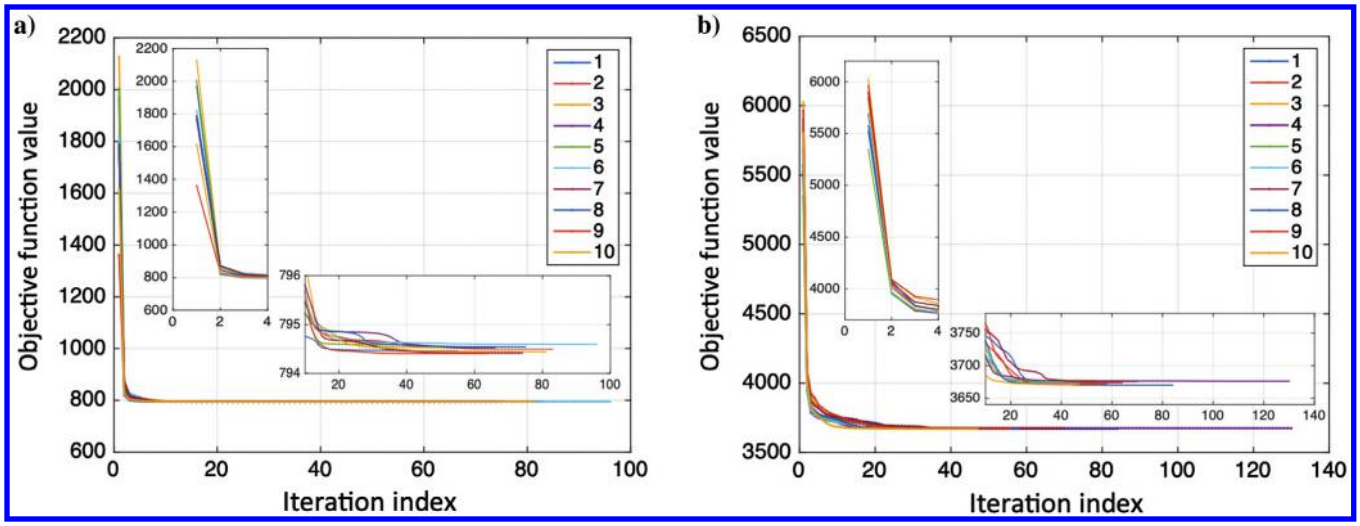

Figure 9. Illustrations of the minimization process using different colors for each optimization with different random initializations for (a) cluster 1 and (b) cluster 2 using data from channel NOLCZ. The magnified panels show details of how the values of the objective function change with iteration number at the beginning and end of each optimization. The objective function is given in equation 10.

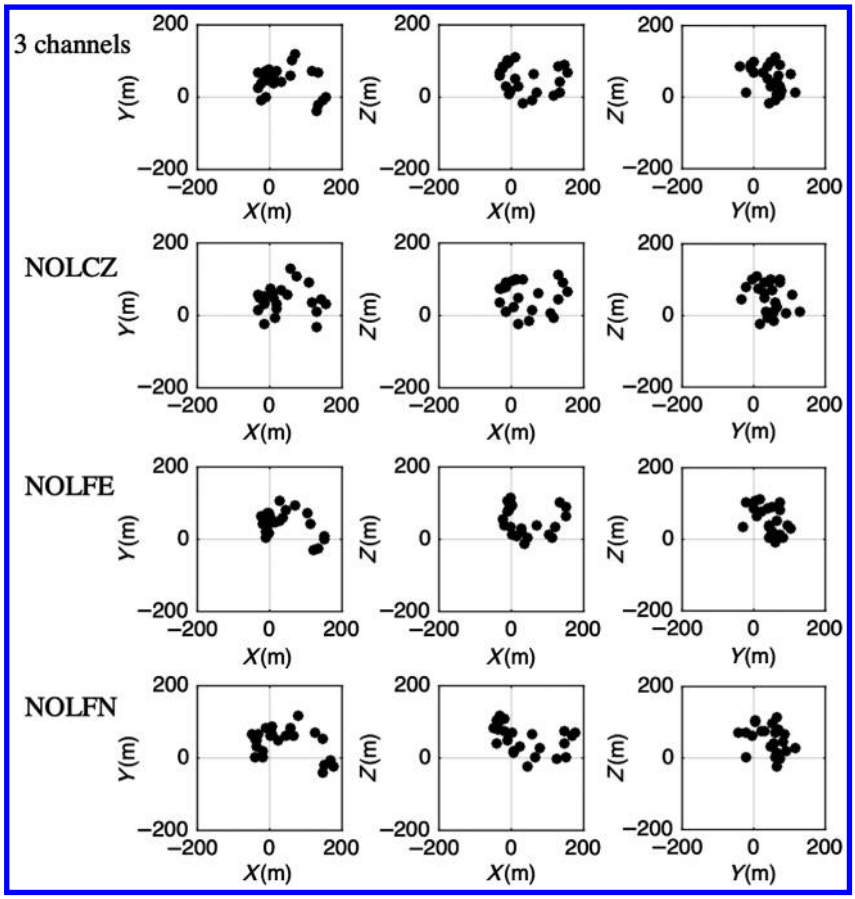

Figure 11. Planar projections of relative event location results of cluster 2, using all three channels (top row) and using single channels NOLCZ, NOLFE, and NOLFN (successive rows). Axes x, y, and z point in orthogonal directions.

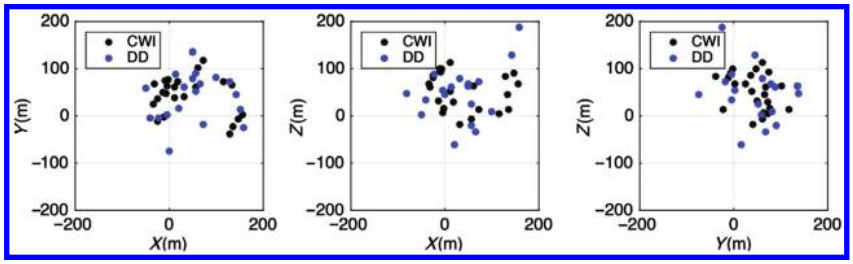

Figure 12. Comparison of the location results of cluster 2 using CWI (black) and DD (blue) methods with data from 3 and 11 station channels.

CONCLUSION

We present a MATLAB package that estimates relative source locations using source separations estimated with the CWI technique. The location method takes account of known biases in CWI separation estimates, and it is capable of correcting them to a significant extent. It is able to locate events with a single station channel as demonstrated in our synthetic and real-data examples and also to combine data from seismic arrays. The code package that accompanies this paper provides a main script that allows users to conduct the three-step method (classifying events, estimating source separations, and estimating relative source locations) while maintaining flexibility for users to edit the code based on their own needs. This computationally inexpensive code can be run on a standard laptop for the size of the event cluster demonstrated herein.

ACKNOWLEDGMENTS

We thank J. Singh (University of Edinburgh) for his constructive reviews of this document and code usability. We also thank B. Baptie (BGS) for providing the seismic data of the New Ollerton earthquakes used in the real-data example.

DATA AND MATERIALS AVAILABILITY

Data associated with this research are available and are included in the code package accompanying this article (downloadable at http://software.seg.org/2019/0007).

REFERENCES

Bai, L., I. Kawasaki, T. Zhang, and Y. Ishikawa, 2006, An improved double-difference earthquake location algorithm using s P phases: Application to the foreshock and aftershock sequences of the 2004 earthquake offshore of the Kii peninsula, Japan (Mw=7.5): Earth, Planets and Space, **58**, 823–830, doi: 10.1186/BF03351987.

Baptie, B. J., 2010, Lava dome collapse detected using passive seismic interferometry: Geophysical Research Letters, **37**, L00E10, doi: 10.1029/2010GL042489.

Brenguier, F., M. Campillo, C. Hadziioannou, N. M. Shapiro, R. M. Nadeau, and E. Larose, 2008b, Postseismic relaxation along the San Andreas fault at Parkfield from continuous seismological observations: Science, **321**, 1478–1481, doi: 10.1126/science.1160943.

Brenguier, F., N. M. Shapiro, M. Campillo, V. Ferrazzini, Z. Duputel, O. Coutant, and A. Nercessian, 2008a, Towards forecasting volcanic eruptions using seismic noise: Nature Geoscience, **1**, 126–130, doi: 10.1038/ngeo104.

Chen, K. H., R. Bürgmann, and R. M. M. Nadeau, 2013, Do earthquakes talk to each other: Triggering and interaction of repeating sequences at Parkfield: Journal of Geophysical Research: Solid Earth, **118**, 165–182, doi: 10.1029/2012JB009486.

de Angelis, S., 2009, Seismic source displacement by coda wave interferometry at Soufrière Hills Volcano, Montserrat, WI: Natural Hazards and Earth System Science, **9**, 1341–1347, doi: 10.5194/nhess-9-1341-2009.

Deichmann, N., and M. Garcia-Fernandez, 1992, Rupture geometry from high-precision relative hypocenter locations of microearthquake clusters: Geophysical Journal International, **110**, 501–517, doi: 10.1111/j.1365-246X.1992.tb02088.x.

Dosso, S. E., and M. J. Wilmut, 2009, Bayesian ocean acoustic source track with environmental uncertainty: Journal of the Canadian Acoustical Association, **37**, 112–113.

Dosso, S. E., and M. J. Wilmut, 2011, Bayesian localization of multiple ocean acoustic sources with environmental uncertainties: Journal of the Canadian Acoustical Association, **39**, 206–207.

Frankel, A. D., C. S. Mueller, T. P. Barnhard, E. V. Leyendecker, R. L. Wesson, S. C. Harmsen, F. W. Klein, D. M. Perkins, N. C. Dickman, S. L. Hanson, and M. G. Hopper, 2000, USGS National seismic hazard maps: Earthquake spectra: Professional Journal of the Earthquake Engineering Research Institute, **16**, 1–19.

Fremont, M., and S. D. Malone, 1987, High precision relative locations of earthquakes at Mount St. Helens, Washington: Journal of Geophysical Research: Solid Earth, **92**, 10223–10236, doi: 10.1029/JB092iB10p10223.

Ge, M. C., 2005, Efficient mine microseismic monitoring: International Journal of Coal Geology, **64**, 44–56, doi: 10.1016/j.coal.2005.03.004.
Gerstenberger, M. C., S. Wiemer, L. M. Jones, and P. Reasenberg, 2005, Real-time forecasts of tomorrow's earthquakes in California: Nature, **435**, 328–331, doi: 10.1038/nature03622.
Got, J. L., J. Frechet, and F. W. Klein, 1994, Deep fault plane geometry inferred from multiplet relative relocation beneath the south flank of Kilauea: Journal of Geophysical Research: Solid Earth, **99**, 15375–15386, doi: 10.1029/94JB00577.
Gret, A., R. Snieder, R. Aster, and P. Kyle, 2005, Monitoring rapid temporal change in a volcano with coda wave interferometry: Geophysical Research Letters, **32**, L06304, doi: 10.1029/2004GL021143.
Gret, A., R. Snieder, and J. Scales, 2006, Time-lapse monitoring of rock properties with coda wave interferometry: Journal of Geophysics Research, **111**, B03305, doi: 10.1029/2004JB003354.
Grigoli, F., S. Cesca, L. Krieger, M. Kriegerowski, S. Gammaldi, J. Horalek, E. Priolo, and T. Dahm, 2016, Automated microseismic event location using master-event waveform stacking: Scientific Reports, **6**, 25744, doi: 10.1038/srep25744.
Helffrich, G., J. Wookey, and I. Bastow, 2013, The seismic analysis code: A primer and user's guide: Cambridge University Press.
Irons, T., 2005, Marmousi2 Model, http://www.reproducibility.org/RSF/book/data/marmousi2/paper.pdf, accessed 15 May 2017.
Ito, A., 1985, High resolution relative hypocenters of similar earthquakes by cross-spectral analysis method: Journal of Physics of the Earth, **33**, 279–294, doi: 10.4294/jpe1952.33.279.
Kawaguchi, E., and N. Fukuda, 2017, "Listening" drone helps find victims needing rescue in disasters, https://www.titech.ac.jp/english/news/2017/040159.html, accessed 15 January 2018.
Kumar, A., E. Zorn, R. Hammack, and W. Harbert, 2017, Seismic monitoring of hydraulic fracturing activity at the Marcellus shale energy and environment laboratory (MSEEL) site, West Virginia: Unconventional Resources Technology Conference, doi: 10.15530/urtec-2017-2670481.
Larose, E., J. de Rosny, L. Margerin, D. Anache, P. Gouedard, M. Campillo, and B. van Tiggelen, 2006, Observation of multiple scattering of kHz vibrations in a concrete structure and application to monitoring weak changes: Physical Review E, **73**, 016609, doi: 10.1103/PhysRevE.73.016609.
Mae, N., Y. Mitsui, S. Makino, D. Kitamura, N. Ono, T. Yamada, and H. Saruwatari, 2017, Sound source localization using binaural difference for hose-shaped rescue robot: Asia-Pacific Signal and Information Processing Association Annual Summit and Conference, 1621–1627.
Martin, G. S., K. J. Marfurt, and S. Larsen, 2002, Marmousi-2: An update model for the investigation of AVO in structurally complex area: 72nd Annual International Meeting, SEG, Expanded Abstracts, 1979–1982, doi: 10.1190/1.1817083.
Marzocchi, W., and A. M. Lombardi, 2008, A double branching model for earthquake occurrence: Journal of Geophysical Research, **113**, B08317, doi: 10.1029/2007JB005472.
Mordret, A., A. D. Jolly, Z. Duputel, and N. Fournier, 2010, Monitoring of phreatic eruptions using interferometry on retrieved cross-correlation function from ambient seismic noise: Results from Mt. Ruapehu, New Zealand: Journal of Volcanology and Geothermal Research, **191**, 46–59, doi: 10.1016/j.jvolgeores.2010.01.010.
Navon, I. M., and D. M. Legler, 1987, Conjugate-gradient methods for large-scale minimization in meteorology: Monthly Weather Reviews, **115**, 1479–1502, doi: 10.1175/1520-0493(1987)115<1479:CGMFLS>2.0.CO;2.
Ottemoller, L., P. Voss, and J. Havskov, 2017, Seisan: Earthquake analysis software for Windows, Solaris and Macosx, http://seisan.info, accessed 20 December 2017.
Press, W. H., B. P. Flannery, S. A. Teukolsky, and W. T. Vetterling, 1987, Numerical recipes: The art of scientific computing: Cambridge University Press.
Ratdomopurbo, A., and G. Poupinet, 1995, Monitoring a temporal change of seismic velocity in a volcano — Application to the 1992 eruption of Mt-Merapi (Indonesia): Geophysical Research Letters, **22**, 775–778, doi: 10.1029/95GL00302.
Roberts, P. M., W. S. Phillips, and M. C. Fehler, 1992, Development of the active doublet method for measuring small velocity and attenuation changes in solids: Journal of the Acoustical Society of America, **91**, 3291–3302, doi: 10.1121/1.402864.
Robinson, D. J., M. Sambridge, and R. Snieder, 2011, A probabilistic approach for estimating the separation between a pair of earthquakes directly from their coda waves: Journal of Geophysical Research, **116**, 1–14, doi: 10.1029/2010JB007745.
Robinson, D. J., M. Sambridge, R. Snieder, and J. Hauser, 2013, Relocating a cluster of earthquakes using a single seismic station: Bulletin of the Seismological Society of America, **103**, 3057–3072, doi: 10.1785/0120130004.
Robinson, D. J., R. Snieder, and M. Sambridge, 2007, Using coda wave interferometry for estimating the variation in source mechanism between double couple events: Journal of Geophysical Research: Solid Earth, **112**, B12302.
Sgattoni, G., O. Gudmundsson, P. Einarsson, and F. Lucchi, 2016, Joint relative relocation of earthquakes without a predefined velocity model: An example from a peculiar seismic cluster on Katla volcano's south-flank (Iceland): Geophysical Journal International, **207**, 1244–1257, doi: 10.1093/gji/ggw331.
Sheng, X., and Y. Hu, 2005, Maximum likelihood multiple-source localization using acoustic energy measurements with wireless sensor networks: IEEE Transactions on Signal Processing, **53**, 44–53.
Snieder, R., 1999, Imaging and averaging in complex media in diffuse waves in complex media: Springer.
Snieder, R., 2006, The theory of coda wave interferometry: Pure and Applied Geophysics, **163**, 455–473, doi: 10.1007/s00024-005-0026-6.
Snieder, R., A. Gret, H. Douma, and J. Scales, 2002, Coda wave interferometry for estimating nonlinear behavior in seismic velocity: Science, **295**, 2253–2255, doi: 10.1126/science.1070015.
Snieder, R., and M. Vrijlandt, 2005, Constraining the source separation with coda wave interferometry: Theory and application to earthquake doublets in the Hayward fault, California: Journal of Geophysical Research, **110**, B04301, doi: 10.1029/2004JB003317.
Stahler, S. C., C. Sens-Schonfelder, and E. Niederleithinger, 2011, Monitoring stress changes in a concrete bridge with coda wave interferometry: The Journal of the Acoustical Society of America, **129**, 1945–1952, doi: 10.1121/1.3553226.
Verlinden, C. M. A., J. Hodgkiss, and W. A. Kuperman, 2015, Passive acoustic source localization using sources of opportunity: The Journal of the Acoustical Society of America, **138**, EL54, doi: 10.1121/1.4933689.
Versteeg, R., 1994, The Marmousi experience: Velocity model determination on a synthetic complex data set: The Leading Edge, **13**, 927–936, doi: 10.1190/1.1437051.
Waldhauser, F., 2001, hypoDD — A program to compute double-difference hypocenter locations: U.S. Geological Survey, https://nehrpsearch.nist.gov/static/files/USGS/PB2006105370.pdf, accessed 10 April 2016.
Waldhauser, F., and W. L. Ellsworth, 2000, A double-difference earthquake location algorithm: Method and application to the northern Hayward fault, California: Bulletin of the Seismological Society of America, **90**, 1353–1368, doi: 10.1785/0120000006.
Waldhauser, F., W. L. Ellsworth, and A. Cole, 1999, Slip-parallel lineations on the Northern Hayward Fault, California: Geophysical Research Letters, **26**, 3525–3528, doi: 10.1029/1999GL010462.
Wang, B., P. Zhu, Y. Chen, F. Niu, and B. Wang, 2008, Continuous subsurface velocity measurement with coda wave interferometry: Journal of Geophysical Research: Solid Earth, **113**, B12313, doi: 10.1029/2008JE003126.
Wegler, U., B. G. Luhr, R. Snieder, and A. Ratdomopurbo, 2006, Increase of shear wave velocity before the 1998 eruption of Merapi volcano (Indonesia): Geophysical Research Letters, **33**, L09303, doi: 10.1029/2006GL025928.
Zhao, Y., A. Curtis, and B. Baptie, 2017, Locating micro-seismic sources with a single seismometer channel using coda wave interferometry: Geophysics, **82**, no. 3, A19–A24, doi: 10.1190/geo2016-0404.1.